communications earth & environment

Article

https://doi.org/10.1038/s43247-024-01271-4

Rapid decrease of the Labrador Sea's influence on black spruce ecosystems with distance inland

Julien Larose[1,7], Étienne Boucher[1,7] ✉, Anne de Vernal[2,7], Ignacio Hermoso de Mendoza[1], Fabio Gennaretti[3], Aliénor Lavergne[4], Laia Andreu-Hayles[5] & Robert D. Field[6]

In eastern Canada, Black spruce (*Picea mariana* Mill. B.S.P.) grows in a wide variety of climates, from maritime-oceanic conditions near the Labrador Sea, to more continental climates, inland. Along this gradient, timing and provenance of heat and moisture that support growth are uncertain, weakening our capacity to predict the response of boreal ecosystems to climate variability. Here, we measured the stable oxygen isotopic composition of black spruce tree-ring cellulose at three sites in eastern Canada and provide evidence of a rapid decrease of Labrador Sea's influence on adjacent ecosystems. Our results report a landwards decrease in the oxygen isotope composition of both tree-ring cellulose ($\delta^{18}O_{TRC}$) and precipitation water ($\delta^{18}O_p$). We also reveal a rapid landwards decoupling between $\delta^{18}O_{TRC}$ variability (1950-2013), maximum temperature and Sea Surface Temperature variations over the Northwest Atlantic. Thus, despite their apparent ecological homogeneity, eastern Canada's black spruce ecosystems rely on heterogeneous sources of heat and moisture.

Labrador Sea is a region of deep water formation that drives decadal climate variability in the North Atlantic[1]. Deep waters formed in this sector contribute significantly to the strengthening of the Atlantic Meridional Overturning Circulation (AMOC), with important consequences on climate variability and sea surface temperatures (SSTs)[2]over the whole circum-Atlantic region, and beyond[3,4]. Because of the magnitude and significance of ocean-atmosphere heat and moisture exchanges, one should expect a detectable influence of the Labrador Sea on land ecosystem dynamics. Indeed, in the taiga forest sector of eastern North-America (above 51°N), multiple lines of evidence suggest that temperature-sensitive black spruce (*Picea mariana* (Mill.) B.S.P.) growth variations are teleconnected to ocean–atmosphere interactions in the Northwest Atlantic[5–7].

However, the extent of the Labrador Sea's direct influence on adjacent black-spruce-dominated forests remains poorly constrained spatially. Easternmost land masses located close to the Labrador Sea exhibit cold maritime-oceanic conditions[8]. By contrast, westernmost land masses are far more continental[8]. For instance, along this gradient, Nishimura and Laroque[9] observed that black spruce tree growth from stands located close to the Labrador Sea responded to July temperatures, while those located inland (>330 km away from the Labrador Sea) revealed a spatially-coherent response to early (May, June) and late (August) growing season temperatures. The longitudinal East-West shift in black spruce's response was thought to reflect a bio-climatic continentality gradient that increases constraints on black spruce growth, landwards[9]. Across such a continentality gradient, sites located close to the Labrador Sea are expected to get a larger proportion of incoming heat and moisture from a direct oceanic influence. This assumption needs to be better verified especially because westerlies redistribute heat and moisture over much of continental and oceanic regions of Northeastern America. Therefore, any influence from the Northwest Atlantic on inland Canadian climate and ecosystems implies westward transport from the Labrador Sea, in spite of prevailing westerly winds. In order to clarify the extent of this influence, alternative proxies more evocative of a direct oceanic imprint on nearby forest dynamics need to be developed.

Stable oxygen isotopes composition ($\delta^{18}O$) may help determining the spatial extent of the influence of Northwest Atlantic / Labrador Sea air

[1]Department of Geography, GEOTOP and Centre d'études nordiques, Université du Québec à Montréal, Montréal, H2X 3R9, Québec, Canada. [2]Department of Earth and Atmospheric Sciences and GEOTOP, Université du Québec à Montréal, Montréal, H2X 3R9, Québec, Canada. [3]Institut de Recherche sur les Forêts and Groupe de Recherche en Écologie de la MRC d'Abitibi, Université du Québec en Abitibi-Témiscamingue, Amos, J9T 2L8, Québec, Canada. [4]Carbon Cycle Research Group, Space and Atmospheric Physics, Imperial College London, London SW7 2AZ, UK. [5]Tree-Ring Laboratory, Lamont-Doherty Earth Observatory of Columbia University, Palisades, New York, NY 10964, USA. [6]Department of Applied Physics and Applied Mathematics, NASA Goddard Institute for Space Studies, New York, NY 10025, USA. [7]These authors contributed equally: Julien Larose, Étienne Boucher, Anne de Vernal. ✉e-mail: boucher.etienne@uqam.ca

masses on surrounding forest ecosystems. Air masses that originate from oceanic regions contain water vapor enriched in heavy oxygen isotopes (^{18}O). As air masses progress over cold and continental areas, water vapor condenses and precipitates, resulting in heavy isotopes being preferentially removed (ie. rained-out) as part of the thermo-dependent Raleigh distillation process[10]. Therefore, it is expected that, as the dominance of oceanic air masses declines along the continentality gradient, oxygen isotope composition of precipitation ($\delta^{18}O_p$) should also decrease. Assuming that all other downstream fractionation processes are of equal importance, this depletion should also be captured by the oxygen isotope composition of tree-ring cellulose ($\delta^{18}O_{TRC}$), as trees use oxygen from source water that originates from precipitation to form carbohydrates during photosynthesis.

Since the pioneering work of Libby[11], $\delta^{18}O_{TRC}$ has been frequently used to infer past changes in summer temperatures in northeastern North America[12–14]. Temperature signals are embedded within $\delta^{18}O_{TRC}$, because temperature influences (i) the isotopic signature of source water ($\delta^{18}O_p$), ii) the rate of transpiration, which further affects evaporative enrichment in the leaf[15–17]. Only few studies have used this proxy to track down the extent of oceanic air masses' influence on boreal forests' growth dynamics. Saurer et al.[18] used 30-year blocks from the Northern Eurasian Tree-Ring Project[19] to map the spatial variability of oxygen isotopes over large scales. Based on $\delta^{18}O_{TRC}$, important continentality gradients were highlighted from Norway to central Russia, but the temporal resolution was too coarse to investigate the influence of year-to-year variability on hydro-climate and ocean–atmosphere heat and moisture exchanges. In the Americas, other studies used $\delta^{18}O_{TRC}$ from trees growing in northwestern Canada[13,20], southwest USA[21] or South America[22,23] to investigate teleconnections between conditions that predominate in the Pacific ocean and western forests' dynamics and climate. However, no studies have used $\delta^{18}O_{TRC}$ to track the influence of the Labrador Sea over adjacent forested lands in eastern North-America.

The objective of the present work is to document the spatial extent of Northwest Atlantic air masses as a heat and moisture source that influence the growth of Eastern Canada's black spruce forests. We measured inter-annual variations (1950–2013) in $\delta^{18}O_{TRC}$ in three sites located across an East–West continentality gradient away from the Labrador Sea, in Eastern Canada (Fig. 1a). Our working hypotheses are twofold. First, we hypothesize that $\delta^{18}O_{TRC}$ values will decrease with continentality, due to the rain-out of heavy isotopes, with distance from the coast. Second, $\delta^{18}O_{TRC}$ from forests growing in an oceanic climate will display a strong connection with hydro-climatic conditions that prevail over the Northwest Atlantic region (Labrador Sea).

Results

Continentality gradients: climate and oxygen isotopes time series

For the 1950–2013 period, maximum (Tmax) and minimum (Tmin) temperature as well as precipitation showed distinct variations during DOY 100–250 (Fig. 1b, c). CAN is significantly colder then the two other sites, both in terms of Tmax (Anova, $F = 40.03$, $p < 0.001$; Tuckey $p < 0.001$) and Tmin (Anova, $F = 45.45$, $p < 0.001$; Tuckey $p < 0.001$). It also receives the least amount of yearly precipitation (350 mm on average, Anova, $F = 19.95$, $p < 0.001$; Tuckey $p < 0.001$) compared to other sites which receive higher amounts (412 mm for FER and 425 mm for GB, Tuckey $p = 0.58$)) (Fig. 1d). FER and GB are the two warmest sites. FER depicts slightly warmer Tmax (Anova, $F = 45.45$, $p < 0.001$; Tuckey $p < 0.001$) compared to the two other sites, but GB shows warmer Tmin (Anova, $F = 45.45$, $p < 0.001$; Tuckey $p < 0.001$). Overall, there is a high correlation between all temperature series. For example, correlations between Tmax range from $r = 0.83$ for CAN and GB to $r = 0.92$ for CAN and FER. The correlation between precipitation series is generally lower, ranging from $r = 0.45$ for CAN and GB to $r = 0.73$ for CAN and FER.

At the GB site, Conrad's (1946) continentality index is constrained within the oceanic-maritime domain (Table 1), with less than 10 incursions in the sub-continental domain over the 1950–2013 period (Fig. 1e). The situation at the two other sites (FER, CAN) shows the opposite. Conrad's continentality indexes remain within the boundaries of continental and sub-continental domains, with rare incursions in the oceanic-maritime domain.

Average $\delta^{18}O_{TRC}$ values decrease significantly along the continentality gradient (Anova, F=86.68, $p < 0.001$). Mean $\delta^{18}O_{TRC}$ values are

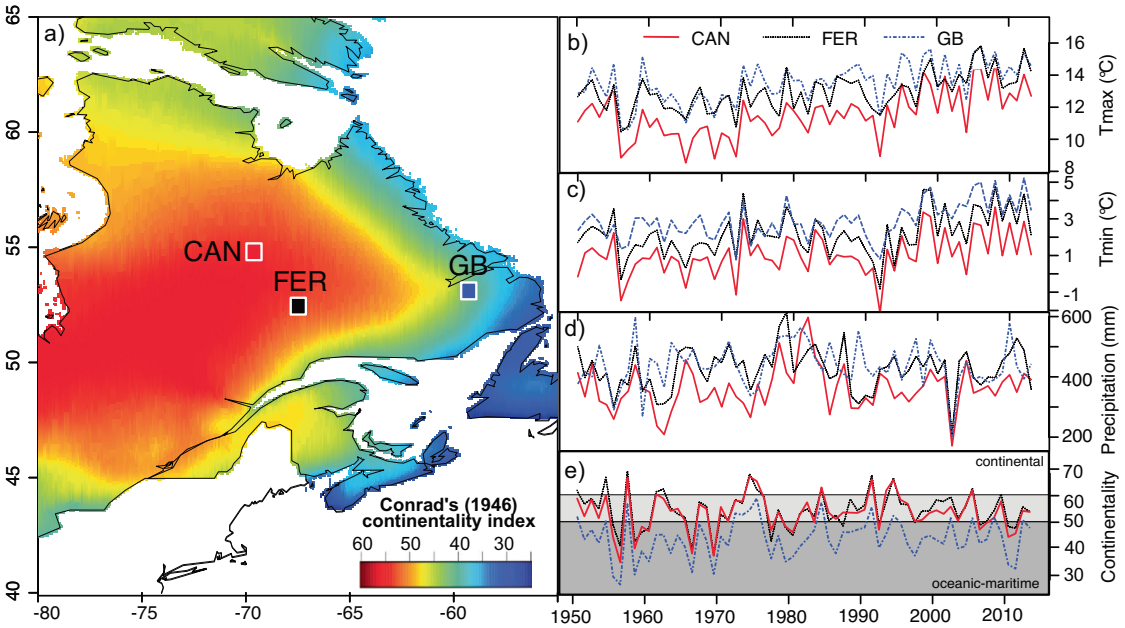

Fig. 1 | Continentality and hydroclimatic gradients in Eastern Canada. Continentality (**a**, **e**) and hydro-climatic (**b**–**d**) gradients in Eastern Canada. **a** Location of the three study sites: Caniapiscau (CAN), Fermont (FER) and Goose Bay (GB). The background map depicts Conrad's (1946) continentality index. On the right side, evolution of **b** maximum (Tmax) and **c** minimum temperature (Tmin) as well as **d** precipitation over the 1950–2013 period, for DOY 100–250. Inter-annual variations in Conrad's (1946) continentality index are shown on (**e**). Gray shading refers to Conrad's 1946 threshold values: 0–50: oceanic maritime; 50–60: sub-continental; 60–100: continental. Map base was retrieved from R CRAN's[50] base package.

24.23 ± 0.84‰, 23.16 ± 0.89‰ and 22.09 ± 1.01‰ at GB, FER, and CAN, respectively (Fig. 2a). The average correlation between all the series is much lower than those of the meteorological time series. GB $\delta^{18}O_{TRC}$ is weakly correlated to both FER ($r = 0.38$) and CAN ($r = 0.18$). In contrast, FER and CAN $\delta^{18}O_{TRC}$ are strongly correlated ($r = 0.55$).

GISS ModelE simulations present $\delta^{18}O_p$ values that also decrease notably with continentality (Fig. 2b). The average seasonal cycle of $\delta^{18}O_p$ shows the highest values near the Labrador Sea (GB site) with mean values reaching −12.5‰ in July (DOY 182 to 212). Comparatively, average peak $\delta^{18}O_p$ values during the same period are −15.2‰ and −16.77‰ in FER and CAN, respectively. This depletion in heavy oxygen isotope composition is also present all year-round at the two most continental sites. FER $\delta^{18}O_p$ is 1.6 ± 0.4‰ heavier on average compared to CAN $\delta^{18}O_p$, and GB $\delta^{18}O_p$ is 3.6 ± 1.3‰ heavier than precipitation at FER.

Regional daily correlations with climate

Correlation coefficients between $\delta^{18}O_{TRC}$ and Tmax are similar among sites, with r values exceeding the critical significance threshold ($r = 0.21, p \leq 0.05$), between DOY 100 and 250 (Fig. 3). FER and CAN depict similar patterns, with peak correlations centered around DOY and 188, 200, respectively. Correlations exceed the critical threshold between DOY 154–212 at FER and DOY 155–239 at CAN. The time window with correlations that exceed the significance threshold is longer at GB, and extends between DOY 100–250, with a peak correlation occurring earlier than for the two continental sites (day 177, $r = 0.51$).

The geographical domains that represent the relationships between $\delta^{18}O_{TRC}$ and Tmax differ for each site, and between seasons. During spring (DOY 100–180), $\delta^{18}O_{TRC}$ in CAN and FER are poorly correlated with regional temperatures, with significant relationships rarely exceeding $r = 0.2$. over much of eastern Canada (Fig. 4). Contrastingly, $\delta^{18}O_{TRC}$ in GB reveals a correlation pattern with regional Tmax that strengthens eastwards, peaking near the Labrador Sea Coast. During summer (DOY 180–250), geographical domains show a larger spatial coverage in all sites, but also show a distinct correlation pattern that unveils significant relationships with Tmax accross western and south-western Canada.

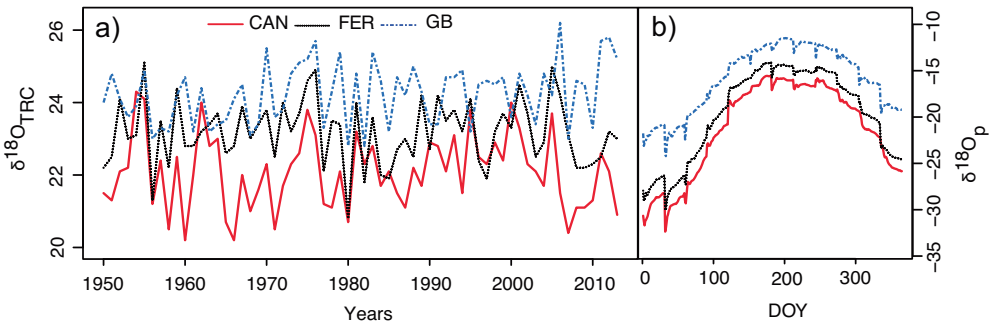

Fig. 2 | Oxygen isotopes in tree rings and precipitation. Oxygen isotopes in tree rings ($\delta^{18}O_{TRC}$, **a**) and in average daily precipitation ($\delta^{18}O_p$, **b**) in Caniapiscau (CAN), Fermont (FER) and Goose Bay (GB) sites (1950–2013). $\delta^{18}O_p$ represents averaged daily $\delta^{18}O_p$ predicted by isotope-enabled GISS modelE, in each of the three sites.

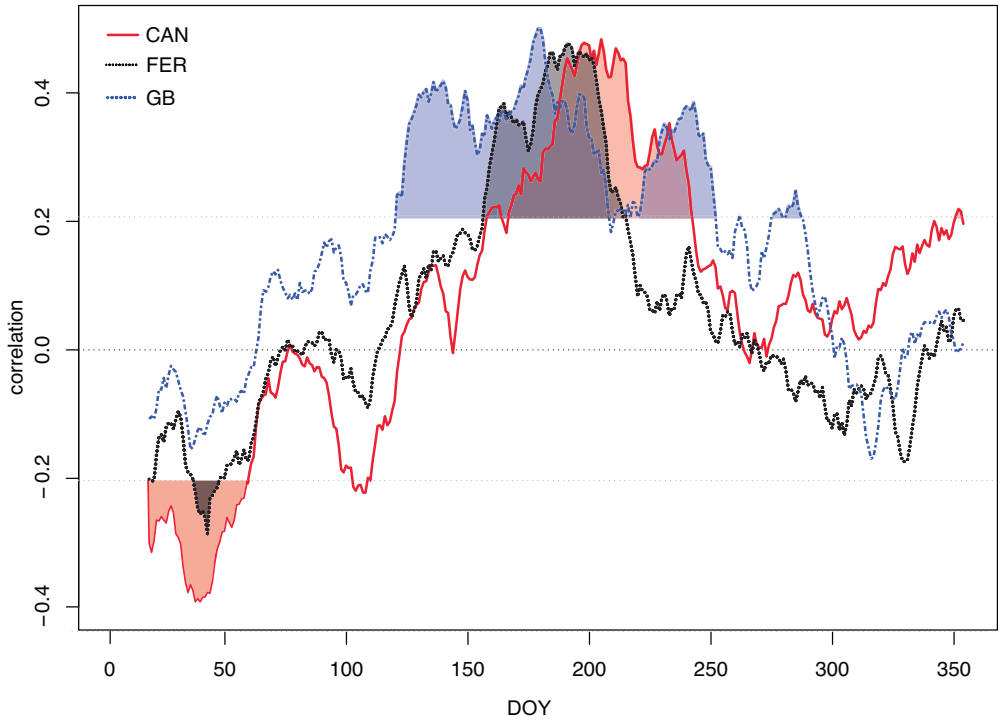

Fig. 3 | Correlations between $\delta^{18}O_{TRC}$ and maximum temperatures. Correlations (Pearson) between $\delta^{18}O_{TRC}$ and local Tmax for each of the three studied sites: Caniapiscau (CAN), Fermont (FER), and Goose Bay (GB). Correlations are performed on daily maximum temperature series using a centered 30-day moving window, moving 1 day at a time.

A strong relationship between $\delta^{18}O_{TRC}$ at GB and west Atlantic conditions is also evident from correlations with North-Atlantic sea surface temperatures (SSTs) during 1950–2013 growing seasons. Indeed, while CAN and FER $\delta^{18}O_{TRC}$ show no particular association with SSTs during this time (Fig. 5), GB $\delta^{18}O_{TRC}$ presents a much stronger, positive and significant geographical pattern of correlations with SSTs in the south of Labrador sea/western Atlantic region.

These spatial patterns are partly reflected in GISS ModelE $\delta^{18}O_p$ simulations (Fig. 6). Geographical domains of correlations between site-specific, precipitation-weighted $\delta^{18}O_p$ and Tmax variability highlight a strong connection with spring temperatures above the Northwest Atlantic/Labrador Sea (DOY 100–180). This connection is clearest for $\delta^{18}O_p$ at the GB site, during spring. During summer (DOY 180–250), correlations between $\delta^{18}O_p$ and Northwest Atlantic/Labrador Sea Tmax variability weaken in all sites (Fig. 6). Instead, $\delta^{18}O_p$ appears to be related to Tmax variability over northwestern parts of the Quebec-Labrador peninsula, at least for the two continental sites, CAN and FER. In GB, $\delta^{18}O_p$ is less correlated with Tmax variability above the North-Atlantic ocean, during summer.

The analysis of 24 h HYSPLIT backward wind trajectories (DOY 100–250, 1960–2013 period, reading at 18:00pm each DOY), for each of the three study sites confirms the existence of a continentality gradient in the

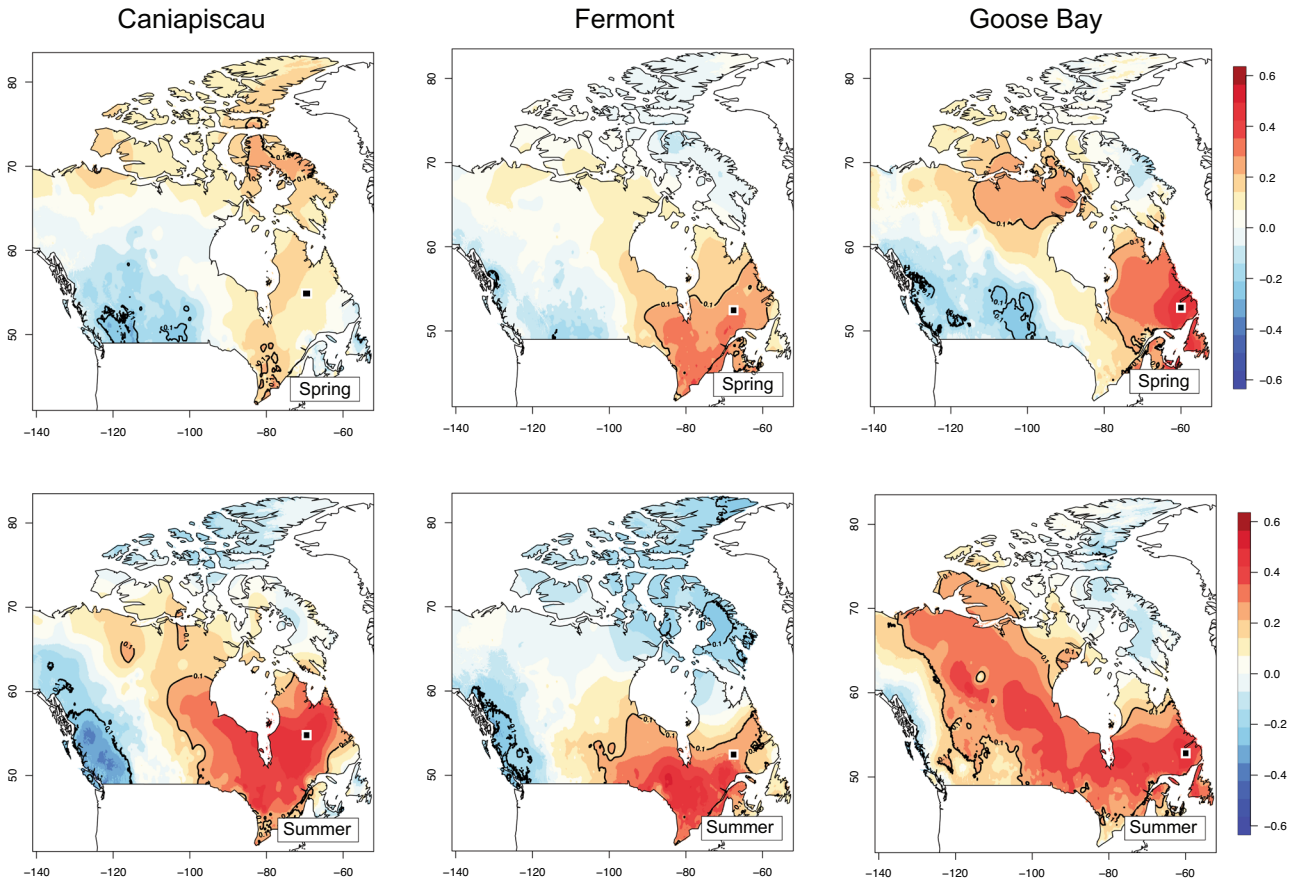

Fig. 4 | Correlations between $\delta^{18}O_{TRC}$ and maximum temperatures during spring and summer. Geographical domains of correlations (Pearson) between site-specific $\delta^{18}O_{TRC}$ and Tmax (data from McKenney et al.[38]) during spring (DOY 100-180, top row) and summer (DOY 180–250, bottom row). Correlations that are significant at the 90% level are shown by the black contour lines. Study sites are indicated by dots on each map. Map base was retrieved from R CRAN's[50] base package.

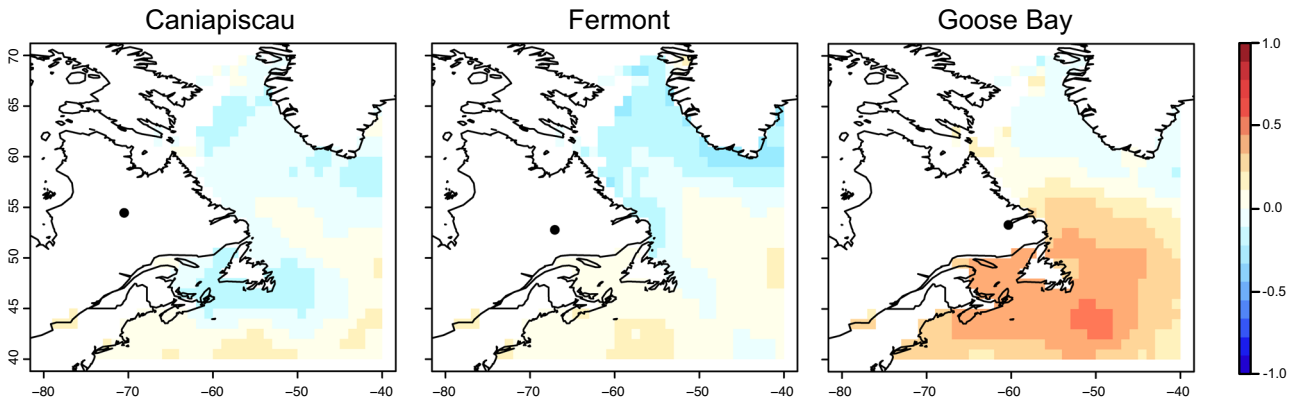

Fig. 5 | Correlations between $\delta^{18}O_{TRC}$ and Northwest-Atlantic sea surface temperatures. Map of correlations (Pearson) between sea surface temperatures during the growing season (May–September average) and $\delta^{18}O_{TRC}$ at each of the study sites, during the 1950–2013 period. Map base was retrieved from R CRAN's[50] base package.

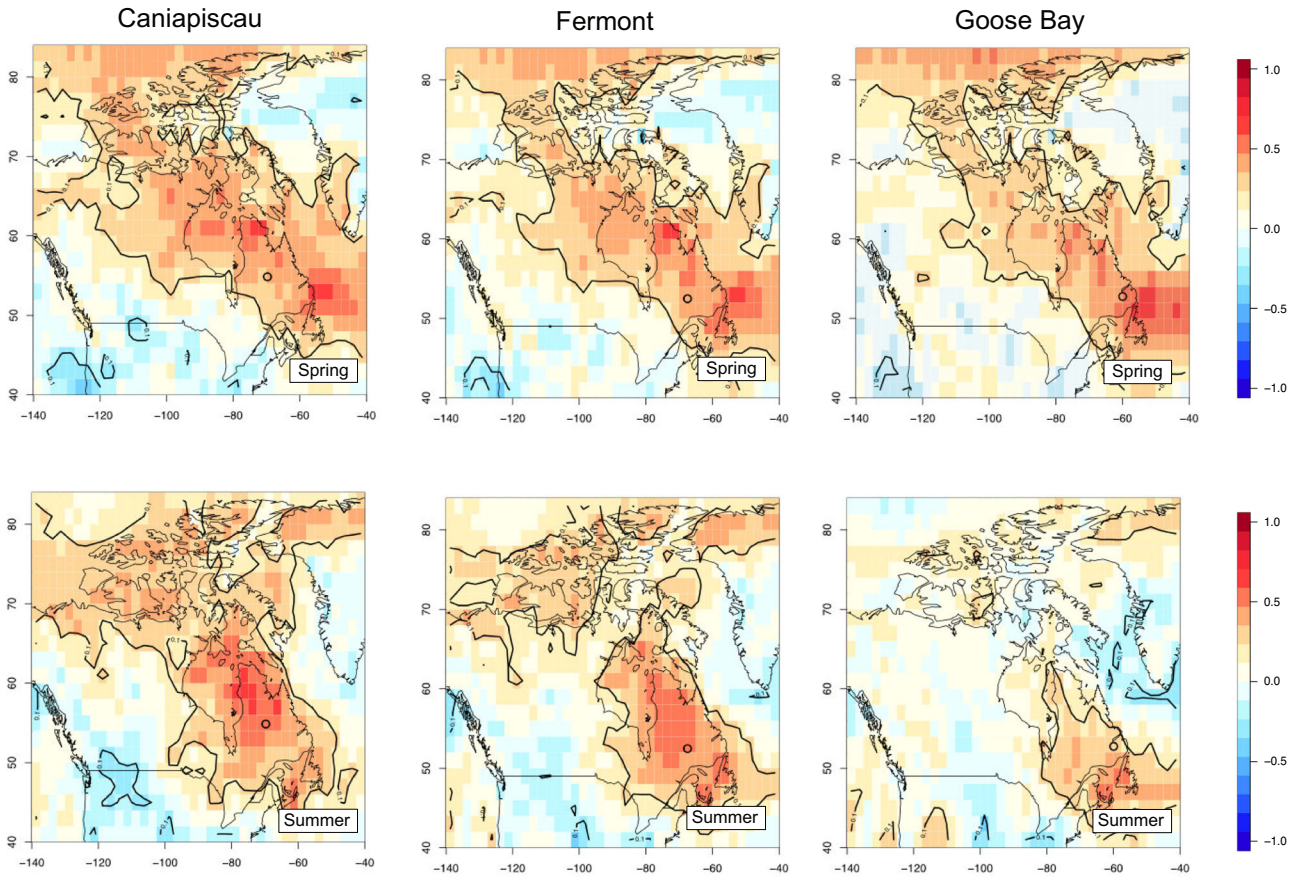

Fig. 6 | Correlations between E-iso modeled $\delta^{18}O_p$ and maximum temperatures during spring and summer. Map of correlations (Pearson) between E-iso-modeled maximum temperatures (Tmax) in the Northwest Atlantic region and E-iso-modeled $\delta^{18}O_p$ (weighted by precipitation) at each of the studied sites. Relationships for spring (first row, DOY 100-180) and summer (second row, DOY 180–250) are represented separately. Correlations that are significant at the 90% level are shown by the black contour lines. Map base was retrieved from R CRAN's[50] base package.

study area (Fig. 7). For example, during spring (DOY 100–180), CAN is exposed to winds originating from all directions, but prevailing winds (68%) are mainly originating from western parts of Quebec-Labrador. In this continental site, only 4% of daily wind sources can be tracked back to the Labrador-Sea/Northwest Atlantic ocean. By contrast, GB is exposed to winds that come predominantly from the North/Northeast, and about 30% of all days experience winds that have an oceanic origin. During summer, this pattern is similar, with westerlies even more apparent for CAN and FER, and 3.5% and 2% winds coming from the Labrador Sea. During the same season, GB receives 29% of its winds from nearby oceanic regions.

Figure 8 shows experiments conducted using the MAIDENiso isotope-enabled ecophysiological model to determine the relative contribution of factors driving changes in the mean $\delta^{18}O_{TRC}$, across the continentality gradient. The two factors to disentangle are : i) changes in leaf-level enrichment (i.e., fractionation during evapotranspiration, primarily controlled by relative humidity, RH) and ii) source water feeding the trees (i.e., primarily controlled by variations in $\delta^{18}O_p$). MAIDENiso experiments suggest that ocean-driven variations in $\delta^{18}O_p$ (i.e., source water), rather than changes in the atmosphere's relative humidity (RH), has the largest influence on the $\delta^{18}O_{TRC}$ simulated by the ecophysiological model. The first three experiments (Fig. 8) were obtained after setting RH to site-specific GB, FER and CAN growing season averages, respectively (all other model inputs set at original CAN values). This yielded no significant changes in the simulated $\delta^{18}O_{TRC}$, along the gradient. By contrast, when setting the source $\delta^{18}O_p$ at site-specific GB, FER and CAN mean annual values, respectively, we noticed a significant −3.5‰ decrease in the average $\delta^{18}O_{TRC}$ simulated by MAIDENiso, suggesting that the source water's oxygen isotopic signature surpasses the effect of RH on mean $\delta^{18}O_{TRC}$ values.

Discussion

In this study, we provide data-based and model-based evidence for a westwards decreasing influence of the Labrador Sea on eastern Canadian boreal forest ecosystems. Among the cornerstones supporting this evidence are (i) an isotopic depletion of $\delta^{18}O_{TRC}$ and $\delta^{18}O_p$ with continentality, (ii) a westwards decoupling of the variability in both isotopic proxy series, with respect to continental Tmax and SST variations over the Northwest Atlantic oceanic region.

The decrease in $\delta^{18}O_{TRC}$ was measured in the tree rings of a single ubiquitous species, black spruce, and matches the landwards depletion of $\delta^{18}O_p$ predicted by the isotope-enabled ModelE (Fig. 2). This confirms our first hypothesis, which postulated that trends in $\delta^{18}O_{TRC}$ should follow the yearly mean isotopic composition of precipitation water. Kurita et al.[24,25] found a similar pattern in Eurasia, where $\delta^{18}O_p$ ratios dropped by more than 15‰ towards continental northeastern Russia. This decrease resulted from the progressive rain-out of moist, oceanic air masses, transported over the Eurasian continent by predominantly westerly winds. In this same region, Saurer et al.[18] noted that $\delta^{18}O_{TRC}$ followed a similar negative trend, and decreased with distance from ocean. Their study was based on long-term $\delta^{18}O_{TRC}$ means (1961–1990) from a large network of sites that included different boreal species. By contrast, our results are based on yearly-resolved analysis of black spruce $\delta^{18}O_{TRC}$ as a single species. In our opinion, this contributes to reducing inter-specific differences, as each species may fractionate oxygen to different rates[26].

Our MAIDENiso experiments (Fig. 8) confirm that variations in the $\delta^{18}O_p$ of source water have the largest effect on the $\delta^{18}O_{TRC}$, along the continentality gradient. Indeed, according to Craig–Gordon's[27] formulation of isotopic fractionation, other factors such as spatial variations in RH, could

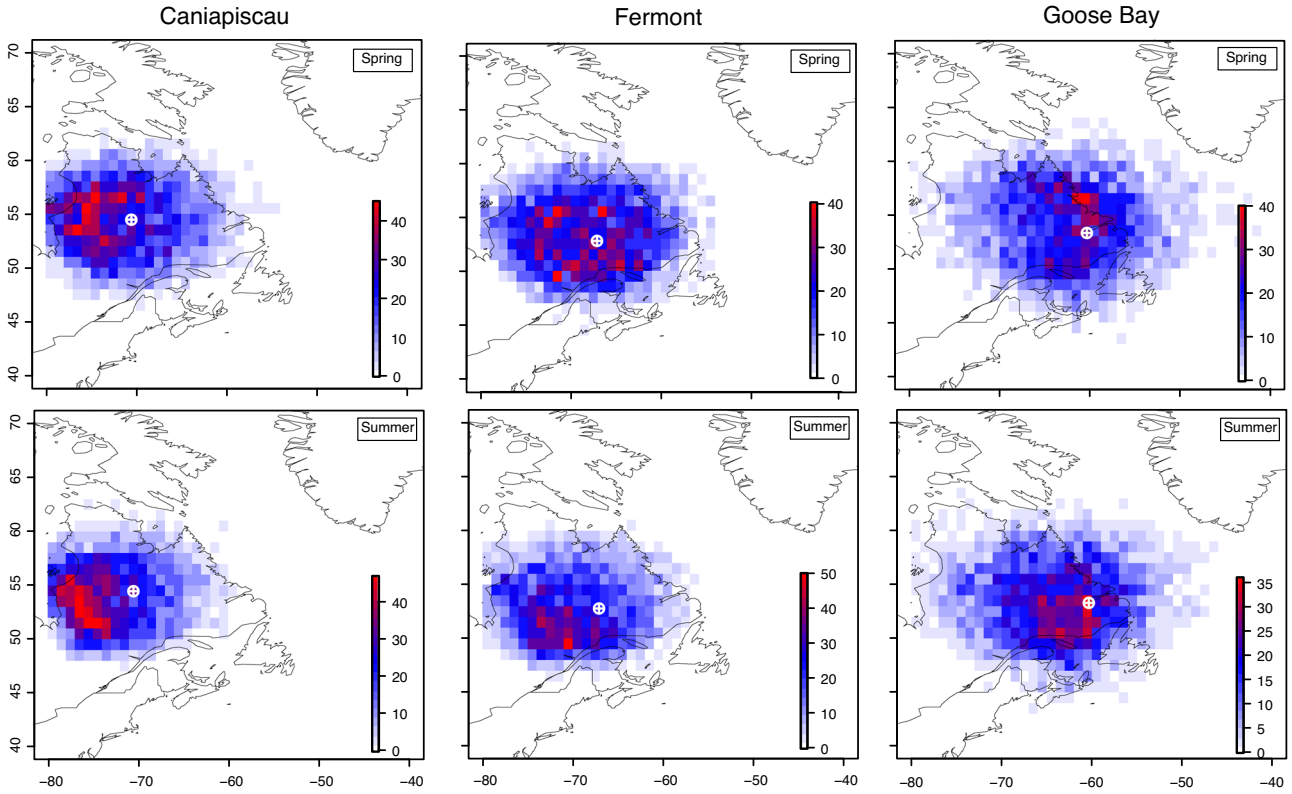

Fig. 7 | HYSPLIT wind back-trajectories during spring and summer. Frequencies of wind daily sources for 24h HYSPLIT[43] back trajectories (reading at 18:00), run for each spring (first row, DOY 100–180) and summer days (second row, DOY 180–250) during the 1960–2013 period. NCEP/NCAR North-American reanalysis[44] data was used as meteorological input for backward HYSPLIT runs, for each of the tree sites.

also trigger landwards depletion in $\delta^{18}O_{TRC}$. However, setting $\delta^{18}O_p$ to site-specific constants along the gradient, yielded reductions in the simulated $\delta^{18}O_{TRC}$ (−3.5‰ between GB and CAN) that are of the same order than those recorded in trees (−2.2‰). Doing the same for RH did not result in noticeable changes in $\delta^{18}O_{TRC}$, although partly because RH itself did not vary substantially during the growing season. Although these experiments cannot replace a thorough, large-scale mechanistic modeling exercise, they still provide preliminary means to move towards the detection / attribution of continentality gradients, mainly through the quantification of the relative effects of $\delta^{18}O_p$ and RH on complex end-products such as $\delta^{18}O_{TRC}$.

Observed $\delta^{18}O_{TRC}$ decrease suggests that the oceanic influence might be limited to the spring season and to the fringe ecosystems located closest to the Labrador Sea shore (Fig. 4). Therefore, this only partly confirms our second hypothesis. During spring, our results indicate an oceanic influence that rapidly fades landwards, with little or no connection between $\delta^{18}O_{TRC}$ and Northwest Atlantic Tmax and SST variability in the most continental sites (FER and CAN). This absence of connection with Northwest Atlantic conditions is also supported by our HYSPLIT backward wind trajectory modeling, which shows that the most continental sites are much less exposed to winds coming from oceanic sources. Instead, these continental sites seem to be preferentially connected to heat and moisture sources that originate from western and southwestern portions of the North American continent, during summer. In the study area, westerlies are the dominant winds that that typically advect moisture and heat along a northwest pathway towards boreal regions of eastern Canada. We hypothesize that, during summer, CAN and FER are predominantly under the influence of such air masses that bring moisture and heat from very distant temperate regions. Along the way, condensation and precipitation favors the depletion of heavy water molecules ($H_2^{18}O$), therefore lowering the composition of $\delta^{18}O_p$ (and $\delta^{18}O_{TRC}$) up to the levels of both continental sites. By contrast, GB seems to be predominantly connected to oceanic air masses originating from the Labrador Sea / Northwest Atlantic region during spring. During this season, warm SSTs in the Labrador Sea region favor evaporation of sea water, transforming these environments into potential sources of heat and moisture for adjacent ecosystems. Enhanced thermo-dependant evaporation yields isotopically enriched water vapor, increasing $\delta^{18}O_p$ and ultimately, $\delta^{18}O_{TRC}$ of trees. Therefore, our analysis shows that oxygen isotopes recorded by trees hold great promise to delineate and quantify ocean-atmosphere interactions in this region.

All $\delta^{18}O_{TRC}$ times series investigated here presented correlations with Tmax that peaked during the growing season (Fig. 3). This overall coherency recalls that $\delta^{18}O_{TRC}$ is an accurate proxy for regional temperature variability. For that reason, it was used in eastern[12,28,29] and western[13,20] Canadian boreal forests to investigate relationships between temperature variability and forest dynamics. However, interestingly, GB is the only site where correlations between $\delta^{18}O_{TRC}$ and Tmax (Fig. 3) are significant during spring (DOY 100–180). This most likely indicates that spring is a preferential period for the occurrence of heat and moisture transfers from the Labrador Sea towards forest ecosystems, on land.

However, the sensitivity of $\delta^{18}O_{TRC}$ in GB during spring, differs slightly from that obtained by Nishimura and Laroque[9], based on tree-ring widths. These authors found, on the contrary, that July (i.e., mid summer) rather than early spring temperatures, exert constraints on black spruce growth in maritime regions of eastern Labrador. However, in their design, ring-width-based response function analyses tend to highlight periods of the year where growth is most limited by climatic conditions. Still, growth may occur outside of these periods, perhaps with lesser constraints imposed by climate. Here, the fact that we find much longer time windows associated with significant $\delta^{18}O_{TRC}$–Tmax correlations probably reflects that reality. Indeed, ocean–atmosphere–vegetation interactions that contribute to the fractionation of oxygen stable isotopes during spring are imprinted in $\delta^{18}O_{TRC}$ records, even in periods of the year where climatic constraints on lateral growth are less marked.

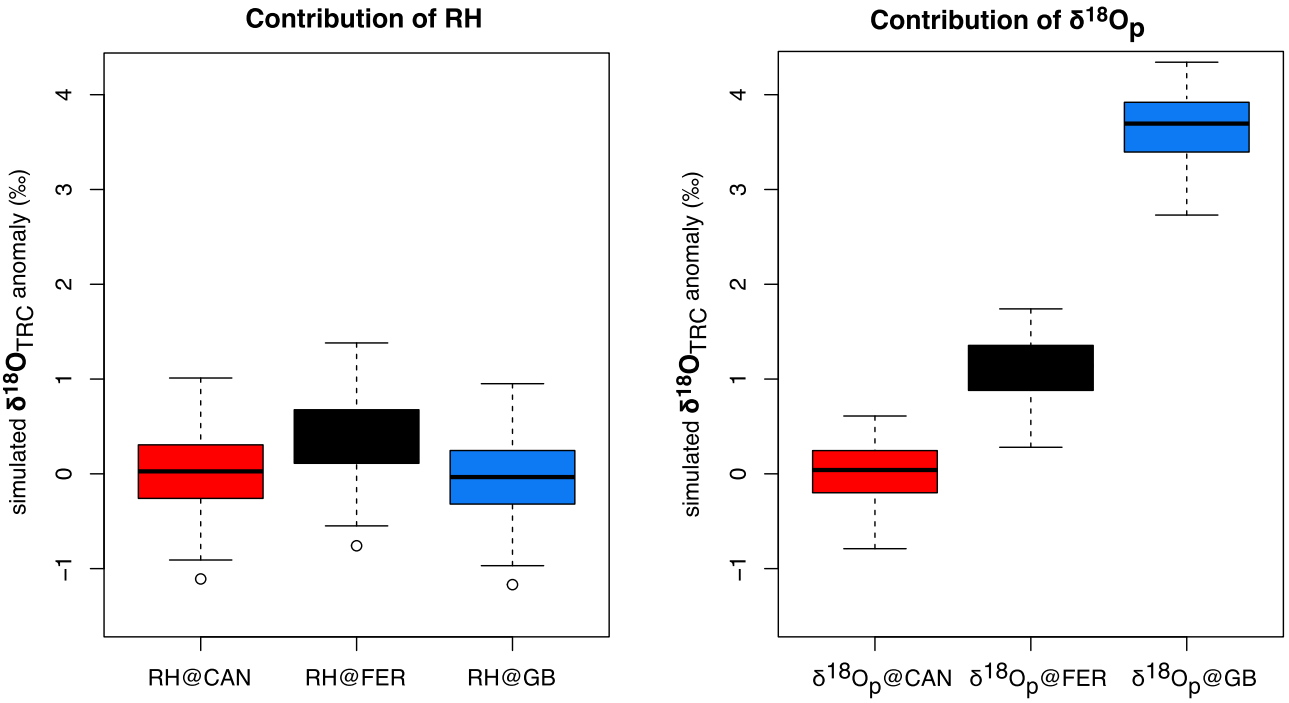

Fig. 8 | MAIDENiso experiments expressing the contributions of relative humidity and $\delta^{18}O_p$ on $\delta^{18}O_{TRC}$. MAIDENiso experiments expressing the contributions of relative humidity (RH) versus $\delta^{18}O_p$ on the average simulated $\delta^{18}O_{TRC}$. Simulated $\delta^{18}O_{TRC}$ values are expressed as ‰ anomalies compared to the Caniapiscau average $\delta^{18}O_{TRC}$, (here set to 0). For each experiment, the MAIDENiso model is parametrized as in[47] for the Caniapiscau site. On the left panel, MAIDENiso simulates $\delta^{18}O_{TRC}$, but with RH set as site-specific constant values. All other variables, including meteorology and $\delta^{18}O_p$, vary on a daily basis, exactly as in the Caniapiscau site. To do this, MAIDENiso uses RH values averaged during the growing season, in each site (CAN = 0.74, FER = 0.72, GB = 0.74). On the right panel, $\delta^{18}O_p$ is assigned as site-specific constants. All other variables, including RH, are allowed to vary on a daily basis, as they do in Caniapiscau. $\delta^{18}O_p$ values correspond to site-specific $\delta^{18}O_p$ averages, retrieved from GISS E-iso model (CAN = −21.95 ‰, FER = −20.33 ‰, GB = −16.59‰). Boxplots represent 0.05, 0.25, 0.50 (middle line), 0.75 and 0.95 quantiles.

We showed, based on isotope-enabled modelE simulations, that interannual variability in $\delta^{18}O_p$ is correlated to Tmax variability over the southern Labrador Sea region, particularly during spring (DOY 100–180) (Fig. 6). Similarly, in Eurasia, continentality gradients favoring rain-out effects are strongest and clearest during the cold season (winter)[25]. By contrast, in summer, continentality gradients are weaker, and the dependence of $\delta^{18}O_p$ on local temperatures is considerably reduced. Indeed, summer conditions favor high evaporation and transpiration rates, leading to greater contributions of water from land surfaces. This results in the mixing (recycling) of water sources and isotopic composition in the atmosphere, a phenomenon that may blur out continentality effects over large scales. In eastern Canada, it is likely that similar seasonal contrasts occur between spring and summer. Continentality gradients required to teleconnect $\delta^{18}O_p$ to Tmax variability over the Labrador Sea region may thus be prominent during spring, a period when water recycling is thought to be minimal.

While ModelE simulations unveiled a teleconnection between site-specific $\delta^{18}O_p$ and Tmax variablity over the Northwest Atlantic during spring, $\delta^{18}O_{TRC}$ recorded this teleconnection only at the GB site. We hypothesize that, during the spring season, black spruce trees located close to the shore benefit from heat and moisture advected from the Labrador Sea, because growth has begun there, and not in other sites. It is important to underline that growing season lengths differ significantly along the continentality gradient. Precise dates for bud burst do not exist, but meteorological records indicate that, in average (1950–2013), GB experiences 770 growing degree days (GDD > 5 °C), with 129 (±11) days above 5 °C. In CAN, these numbers drop to 679 GDD and less then 110 days days above 5 °C. As a supporting evidence, MODIS-derived Enhanced Vegetation Indexes (EVI,[30]) between 2003 and 2023 (DOY 70 to DOY 180, inclusively), also tend to show an earlier inflexion point in the EVI time series in GB (DOY 115) compared to CAN (DOY 130) (Fig. 9). Thus, in GB, the growing season is not only warmer, but also approximately 15 days longer. However, while delays exist in phenology at the scale of the full gradient, $\delta^{18}O_{TRC}$ also differs in mean between GB and FER, even if the two sites present comparable behaviors from the perspective of EVI. This suggest that not only the timing of growth start but also the isotopic signature of source water that feeds the tree, when growth starts, needs to be considered.

In the studied region, heat and moisture transfers may depend on the complex interactions between ocean, atmosphere and sea ice conditions in the area. In the Labrador Sea and across the Eastern Newfoundland coast, sea ice starts forming in January, and reaches its maximum extent at the end of March, on average[31]. Then, under the effect of rising temperatures, the ice cover starts to melt in April (DOY 91–121). By mid-June, the Labrador Sea is typically in open water conditions[32], freeing up an important oceanic region from which surface waters may evaporate and be transported as moist air toward adjacent lands[33]. As such, the length of the ice-free season is, itself, a thermo-dependent process. Therefore, during warm years, sea ice recedes fast, SSTs rise, and more heat may be advected over surrounding boreal forests. Due to these thermo-dependant exchanges, land temperatures are also expected to rise over adjacent forests and precipitation-derived source water for trees becomes enriched in heavy oxygen isotopes (^{18}O), ultimately resulting in higher $\delta^{18}O_{TRC}$ values.

However, sea ice formation and melt in the Labrador Sea region do not solely depend on spring and summer temperatures. In this region, Wang et al.[33] showed that positive North Atlantic Oscillation (NAO) indexes are associated with strengthened westerlies, causing sea ice cover anomalies in winter and spring. Such teleconnections with large-scale atmospheric pressure systems may also introduce significant temporal persistence in the duration of the ice period, up to 10 years, as suggested by Wang et al.[33]. This temporal persistence is exacerbated by the fact that the Labrador Sea waters are in constant interaction with sea surface conditions that prevail in the Baffin Bay and the Greenland Sea. This situation introduces significant amount of complexity in sea ice dynamics, as both oceanic

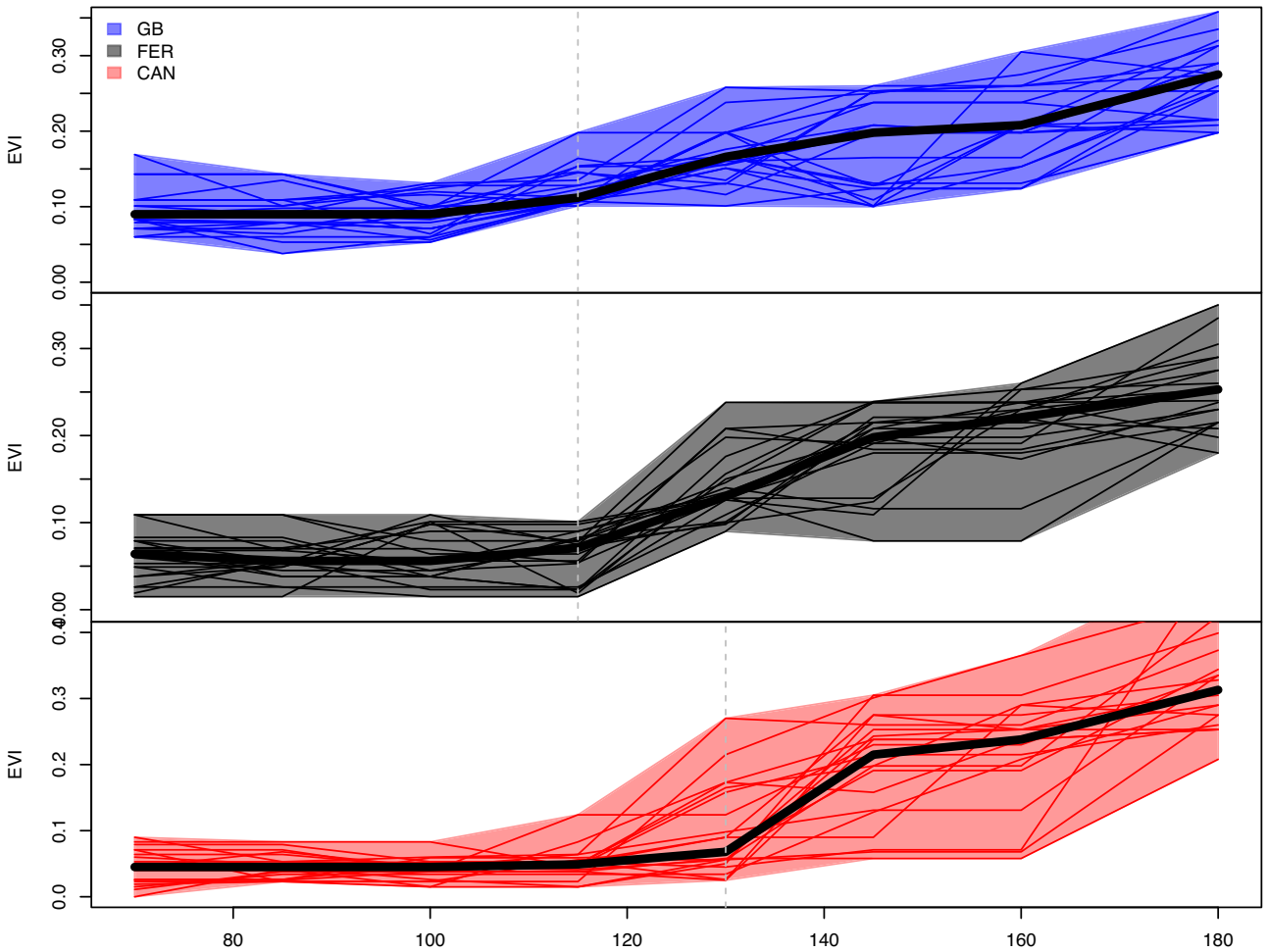

Fig. 9 | MODIS-derived enhanced vegetation indexes along the continentality gradient. MODIS-derived enhanced vegetation indexes (EVI[30]) between 2003 and 2023 (DOY 70–180, inclusively). Dashed vertical lines represent inflexion points in the EVI time series in GB, FER (DOY 115) and CAN (DOY 130). Colored fills are determined using minimum and maximum values, while the bold black line is the median.

and atmospheric forcings are likely to determine the extent, duration and persistence of the ice cover in the Labrador Sea[34,35]. A thorough investigation, based on both an extensive network of $\delta^{18}O_{TRC}$ and a coupled global circulation model would be necessary to refine our understanding of how ocean-atmosphere-ice interactions that prevail in the Labrador Sea during spring, may impact the climate and ecosystems over surrounding lands.

Conclusion

We provide evidence that the Labrador Sea is a source of heat and moisture for trees growing in the easternmost part of the Quebec-Labrador peninsula (GB site). However, the Labrador Sea's influence diminishes landwards very rapidly, being predominant in GB during spring and non-existent in the most continental sites (FER and CAN). This phenomena is illustrated by a decrease in mean $\delta^{18}O_{TRC}$ measured in tree rings from homogeneous, mature black spruce trees sampled along the continentality gradient. The decrease in $\delta^{18}O_{TRC}$ echoes a trend also visible in the signature of source water. As we move inland, precipitation gets increasingly depleted in heavy isotopes, therefore reducing $\delta^{18}O_p$ along the way. This depletion mechanism is represented by the isotope-enabled GISS ModelE, from which variations in the seasonal cycle of $\delta^{18}O_p$ are extracted. This continentality gradient is also characterized by inter-annual variations in $\delta^{18}O_{TRC}$ that are increasingly decoupled from land and sea surface temperature variations that prevail over the Labrador Sea region.

This study suggests that while most high-latitude black spruce forests are sensitive to temperature variations during the growing season, not all sites receive heat and moisture from the same sources and at the same time. It is evident from our $\delta^{18}O_{TRC}$ results, that the most continental sites such as FER and CAN are connected to heat sources that predominantly originate from western parts of the continent. In contrast, at the GB site, the site located closest to the coast, $\delta^{18}O_{TRC}$ variations seem to be in phase with temperature variations observed in the Labrador Sea region, during spring. During this season, the advection of moisture and heat and their transfer to adjacent lands is likely to depend on the extent of the sea ice cover. The sooner the sea ice melts, the longer the period favorable for heat and moisture transfers towards adjacent lands. Based on these large scale ocean-land interactions, our study underlines the fact that changes in heat and water sources need to be taken into account to predict the fate of black spruce forests to climate change. While such forests are often seen as homogeneous ecosystems across much of eastern Canada, our study highlights that significant regional differences exist concerning the sources of heat and moisture that support growth. This finding also has important implications for the interpretation of hydro-climate reconstructions based on $\delta^{18}O_{TRC}$, in the study area. Depending on where reference trees are sampled (continental or maritime regions), sources of heat and moisture affecting $\delta^{18}O_{TRC}$ may differ considerably, impacting both the location, extent and variability of the signal being reconstructed.

Methods

Study sites

Three sites were selected along a gradient of continentality in eastern Canada (Table 1, Fig. 1a). Each site is composed of old, even-aged, mono-specific black spruce *Picea mariana* Mill. forests growing on mesic soils

between 400 and 565 m of altitude (ASL). The first site is located near the town of Goose Bay (GB) in Newfoundland-Labrador (Canada). It is located about 300 km west of the Labrador Sea coast and about 20 km south of the salty Melville Lake, which drains eastwards into the Labrador Sea. The second and third sites are located near the town of Fermont (FER) and near the Caniapiscau (CAN) hydro-electric river dam, respectively. FER is located > 700 km west of the Labrador Sea, while CAN is located >1000 km away from the ocean.

Tree-ring measurements and isotopic analysis

At each site, between 10 and 15 mature black spruce (*Picea mariana* Mill.) trees were sampled for dendrochronological analysis. On each tree, a cross-section was collected at breast height. Back to the lab, rings were counted on two perpendicular radii, measured using CooRecorder, and cross-dated in PAST 5. To facilitate dating, ring width chronologies were standardized and transformed into tree-ring indices (TRI) using a 66% series-length spline in R CRAN's package dplR[36]. Among the trees dated, a subset of five individuals were selected for the analysis of stable oxygen isotopes in tree-ring cellulose. Only trees without reaction wood were considered. Rings were individualized using a scalpel on each of these two radii, back to 1950. The 20 first years of growth were never cut, to avoid including juvenile effects in the isotopic series. Individualized rings were ground and homogenized using a ball mill grinder, and an equal mass of each ring was pooled with other rings of the corresponding years, for each site. α-cellulose, the purest and most stable form of cellulose, was extracted according to standard protocols[37]. The oxygen isotope composition in tree-ring cellulose ($\delta^{18}O_{TRC}$) was measured at the Geotop's stable isotope laboratory. Between 0.3 and 0.4 mg of α-cellulose per year were analyzed with an Isotope Ratio Mass Spectrometer (IRMS, Isoprime VisIon) coupled to an elemental analyzer (Elementar, Vario PyroCube) in continuous flow. The $\delta^{18}O_{TRC}$ composition was expressed in per mil (‰), relatively to the "Vienna Standard Mean Ocean Water" (VSMOW). Measurements were calibrated based on two internal reference materials : $\delta^{18}O = 5.47 \pm 0.04$‰ and 38.95 ± 0.04‰. A third reference ($\delta^{18}O = 29.79 \pm 0.04$‰) was used to quantify analytical precision (±0.3‰).

Correlations with climate data

Based on the $\delta^{18}O_{TRC}$ times series produced for GB, FER and CAN (1950–2013), we analyzed the correlations with local and regional climate variability. For this, we used the interpolated, 10 km × 10 km, daily gridded dataset from Natural Resources Canada[38]. For each site, we extracted daily maximum temperatures (Tmax, °C) and total precipitation (Prec, mm). We then computed daily running correlations (Pearson) between local $\delta^{18}O_{TRC}$ and daily climate variations using a 30-days window, moved iteratively by one day across the whole year. This allowed us to pinpoint periods of the year which were best correlated with the $\delta^{18}O_{TRC}$ measured at each site. For all sites, we focalized on correlations with Tmax, as preliminary analysis revealed that correlations between $\delta^{18}O_{TRC}$ and precipitation were never significant. We also used this same gridded dataset to calculate regional correlation patterns across Canada, taking each of the local $\delta^{18}O_{TRC}$ as reference. To do this, we averaged Tmax variations for two specific time periods: days of year (DOY) 100–180 for spring, and DOY 180–250 for summer. Natural Resources Canada's climate dataset was used to calculate the Conrad's continentality index.[39] for each of the three study sites, and across eastern Canada (Fig. 1a). Conrad's continentality index (K, in %) is expressed as follows: $K = mA/sin\Phi + N$, where A corresponds to the difference (range) between warmest and coldest months, Φ is latitude and m and N are constants (1.7 and −14, respectively). Correlation maps were also performed between $\delta^{18}O_{TRC}$ at each site, and sea surface temperatures (SST) retrieved from[40]. Average SST values during the growing season were calculated from monthly May to September values.

$\delta^{18}O_p$ simulations

The Goddard Institute for Space Studies (GISS)'s ModelE[41] climate model was used to predict, in an idealized sense, the spatio-temporal variability of $\delta^{18}O$ in precipitation ($\delta^{18}O_p$) at each of the three sites. ModelE is equipped with stable water isotope tracers that follow the hydrological cycle with fractionation during each phase change[42]. The simulation was run at the F40 resolution with 40 vertical layers and 2° × 2.5° horizontal resolution. Inter-annually-varying sea surface temperatures (1951–2014) were prescribed along with a free-running atmosphere. First, we used ModelE to predict the mean variations in the seasonal cycle of $\delta^{18}O_p$ across the continentality gradient. We also used simulated $\delta^{18}O_p$ to investigate the relationship between local and regional $\delta^{18}O_p$ variations and Tmax, as simulated in the numerical environment. In order to calculate seasonal means of $\delta^{18}O_p$, we calculated weighted averages using daily precipitation as numerical weights.

HYSPLIT backward wind trajectories

HYSPLIT[43] was used to calculate 24 h backward wind trajectories for each study site, for DOY 100–180 (spring) and DOY 180–250 (summer), during the 1960–2013 period (200 m height, reading at 18:00). NCEP/NCAR reanalysis data[44] were used as meteorological inputs for these runs. For each 24 h backward trajectory, the geographical coordinates of each source points were stored (ie. 54 years × 151 DOY = 8154 source points). The frequency (count) of all these wind source points were then plotted on a 1° resolution raster map, to identify the most prominent wind sources for each site during each season.

MAIDENiso experiments

We used MAIDENiso[45,46], a state-of-the-art isotope-enabled ecophysiological model, to better quantify the relative importance of processes contributing to the end-product, $\delta^{18}O_{TRC}$, recorded in tree rings. This helped us determine, based on an idealized representation of the mechanistic functioning of black spruce trees, if variations in the average $\delta^{18}O_{TRC}$ along the continentality gradient, are best explained by processes occurring at the leaf-level (i.e., fractionation during evapotranspiration, primarily controlled by relative humidity, RH) or by processes affecting variations in the source water feeding the trees (ie.primarily controlled by variations in $\delta^{18}O_p$). Using simple meteorological inputs and CO_2 concentrations, MAIDENiso simulates water and carbon fluxes at the vegetation-atmosphere interface, and accounts for the influence of phenology and carbon allocation strategies while simulating growth of various sinks, such as tree stem. Along this mechanistic chain, MAIDENiso also calculates $\delta^{18}O_{TRC}$ by resolving Danis et al.[46]'s formulation of the Craig–Gordon model[27] at a daily time step, weighting these simulations by daily Gross Primary Production (GPP) in order to obtain yearly records of $\delta^{18}O_{TRC}$. Here, we used a recent calibration

Table 1 | Basic site information and number of trees sampled for dendrochronological analyses

Site name	Dist.from Labrador sea (km)	Altitude ASL (m)	Continentality index (yr-mean)	Mean tree age (yrs)	No. trees sampled (selected for $\delta^{18}O_{TRC}$)
Goose Bay (GB)	300	410	43.9[a]	134	15 (5)
Fermont (FER)	700	530	53.3[b]	94	10 (5)
Caniapiscau (CAN)	1000	565	54.4[b]	150	11 (5)

[a]Oceanic-maritime climate.
[b]Sub-continental climate, as classified by Conrad (1946).

of MAIDENiso for Black spruce trees growing in the CAN site, which was published in a separate work[47]. This calibration was performed using the same Natural Resources Canada meteorological dataset, as used for daily correlation analysis (see above). Daily CO_2 data were obtained from the Mauna Loa Observatory[48] and were corrected with the CarbonTracker measurement and modeling system[49]. Based, on this initial calibration, we produced the following experiments. First, in order to isolate the effect of RH on $\delta^{18}O_{TRC}$, we produced, three different simulations, each time setting RH at site-specific CAN, FER, GB levels (but leaving all other variables as in[47]). For each run, we therefore averaged RH during the growing season (between DOY 100 and 250), based on each site's meteorology, and simulated the respective $\delta^{18}O_{TRC}$. We then conducted a similar experiment, although this time leaving RH free to vary, but setting $\delta^{18}O_p$ to site-specific E-iso yearly-averaged simulated values. All MAIDENiso experiments results were represented as boxplots, and expressed as $\delta^{18}O_{TRC}$ values (‰) relative to Caniapiscau (CAN) simulated levels (CAN $\delta^{18}O_{TRC}$ is centered on zero).

Data availability

$\delta^{18}O_{TRC}$ data produced in this study can be found and downloaded here: https://quebeclabradortr.shinyapps.io/TRdashboard4/#section-stable-isotopes-oxygen. All data used to produce the figures are found here: https://github.com/boucheret/Larose.git

Code availability

The Goddard Institute for Space Studies (GISS) ModelE code used to predict $\delta^{18}O_p$ can be found via this publication https://doi.org/10.1002/2013ms000265. MAIDENiso ecophysiological model's source code, data and calibration can be found here: https://zenodo.org/records/5597877.

Received: 10 March 2023; Accepted: 14 February 2024;
Published online: 28 February 2024

References

1. Ortega, P., Robson, J., Sutton, R. T. & Andrews, M. B. Mechanisms of decadal variability in the Labrador Sea and the wider North Atlantic in a high-resolution climate model. *Clim. Dyn.* **49**, 2625–2647 (2017).
2. Zhang, L. & Wang, C. Multidecadal North Atlantic sea surface temperature and Atlantic meridional overturning circulation variability in CMIP5 historical simulations. *J. Geophys. Res.* **118**, 5772–5791 (2013).
3. Rahmstorf, S. et al. Exceptional twentieth-century slowdown in Atlantic Ocean overturning circulation. *Nat. Clim. Change* **5**, 475–480 (2015).
4. Oldenburg, D., Wills, R. C., Armour, K. C., Thompson, L. & Jackson, L. C. Mechanisms of low-frequency variability in North Atlantic Ocean heat transport and AMOC. *J. Clim.* **34**, 4733–4755 (2021).
5. Boucher, E., Nicault, A., Arseneault, D., Bégin, Y. & Karami, M. Decadal variations in Eastern Canada's taiga wood biomass production forced by ocean-atmosphere interactions. *Sci. Rep*. **7**, 2457 (2017).
6. Nicault, A. et al. Spatial analysis of black spruce (Picea mariana (Mill.) B.S.P.) radial growth response to climate in northern Québec - Labrador Peninsula, Canada. *Can. J. Forest Res*. **45**, 343–352 (2015).
7. Ols, C. et al. Post-1980 shifts in the sensitivity of boreal tree growth to North Atlantic Ocean dynamics and seasonal climate: Tree growth responses to North Atlantic Ocean dynamics. *Glob. Planet. Change* **165**, 1–12 (2018).
8. Barry, R. G. A note on the synoptic climatology of Labrador-Ungava. *Q. J. R. Meteorol. Soc.* **86**, 557–565 (1960).
9. Nishimura, P. H. & Laroque, C. P. Observed continentality in radial growth-climate relationships in a twelve site network in western Labrador, Canada. *Dendrochronologia* **29**, 17–23 (2011).
10. Rozanski, K., Sonntag, C. & Münnich, K. Factors controlling stable isotope composition of European precipitation. *Tellus* **34**, 142–150 (1982).
11. Libby, L. M. et al. Isotopic tree thermometers. *Nature* **11**, 284–288 (1976).
12. Naulier, M. et al. Temporal instability of isotopes-climate statistical relationships—a study of black spruce trees in northeastern Canada. *Dendrochronologia* **34**, 33–42 (2015).
13. Porter, T. J. et al. Spring-summer temperatures since AD 1780 reconstructed from stable oxygen isotope ratios in white spruce tree-rings from the Mackenzie Delta, northwestern Canada. *Clim. Dyn.* **42**, 771–785 (2014).
14. Gennaretti, F. et al. Bayesian multiproxy temperature reconstruction with black spruce ring widths and stable isotopes from the northern Quebec taiga. *Clim. Dyn.* **49**, 4107–4119 (2017).
15. Barbour, M., Roden, J. S., Farquhar, G. D. & Ehleringer, J. R. Expressing leaf water and cellulose oxygen isotope ratios as enrichment above source water reveals evidence of a Peclet effect. *Oecologia* **138**, 426–435 (2004).
16. Barbour, M. Stable oxygen isotope composition of plant tissue: a review. *Funct. Plant Biol.* **34**, 83–94 (2007).
17. Gessler, A. et al. Stable isotopes in tree rings: towards a mechanistic understanding of isotope fractionation and mixing processes from the leaves to the wood. *Tree Physiol.* **34**, 796–818 (2014).
18. Saurer, M., Schweingruber, F., Vaganov, E. A., Shiyatov, S. G. & Siegwolf, R. Spatial and temporal oxygen isotope trends at the northern tree-line in Eurasia. *Geophys. Res. Lett.* **29**, 7–1 (2002).
19. Schweingruber, F. H. Dendrochronological sampling strategies for radiodensitometric networks in northern hemisphere subalpine and boreal zones. *Eur. Palaeoclim. Man* **4**, 205–209 (1993).
20. Field, R. D. et al. Tree-ring cellulose $\delta^{18}O$ records similar large-scale climate influences as precipitation $\delta^{18}O$ in the Northwest Territories of Canada. *Clim. Dyn*. **58**, 1–18 (2021).
21. Johnstone, J. A., Roden, J. S. & Dawson, T. E. Oxygen and carbon stable isotopes in coast redwood tree rings respond to spring and summer climate signals. *J. Geophys. Res.* **118**, 1438–1450 (2013).
22. Rodriguez-Caton, M. et al. Hydroclimate and ENSO variability recorded by oxygen isotopes from tree rings in the South American Altiplano. *Geophys. Res. Lett.* **49**, e2021GL095883 (2022).
23. Brienen, R. J., Helle, G., Pons, T. L., Guyot, J. L. & Gloor, M. Oxygen isotopes in tree rings are a good proxy for Amazon precipitation and El Niño-Southern Oscillation variability. *Proc. Natl Acad. Sci. USA* **109**, 16957–16962 (2012).
24. Kurita, N., Numaguti, A., Sugimoto, A., Ichiyanagi, K. & Yoshida, N. Relationship between the variation of isotopic ratios and the source of summer precipitation in eastern Siberia. *J. Geophys. Res.* **108**, 4339 (2003).
25. Kurita, N., Yoshida, N., Inoue, G. & Chayanova, E. A. Modern isotope climatology of Russia: a first assessment. *J. Geophys. Res.* **109**, D03102 (2004).
26. Reynolds-Henne, C. E., Saurer, M. & Siegwolf, R. T. Temperature versus species-specific influences on the stable oxygen isotope ratio of tree rings. *Trees* **23**, 801–811 (2009).
27. Craig, H. Isotopic variations in meteorics waters. *Science* **133**, 1702–1703 (1961).
28. Naulier, M. et al. Carbon and oxygen isotopes of lakeshore black spruce trees in northeastern Canada as proxies for climatic reconstruction. *Chem. Geol.* **374**, 37–43 (2014).
29. Lavergne, A. et al. Modelling tree ring cellulose $\delta^{18}O$ variations in two temperature-sensitive tree species from North and South America. *Clim. Past* **13**, 1515–1526 (2017).
30. Didan, K. MODIS/Aqua Vegetation Indices 16-Day L3 Global 250m SIN Grid V061. 2021, distributed by NASA EOSDIS Land Processes Distributed Active Archive Center. https://doi.org/10.5067/MODIS/MYD13Q1.061 (2021).
31. Wu, Y. et al. The impact of sea ice on the initiation of the spring bloom on the Newfoundland and Labrador Shelves. *J. Plank. Res.* **29**, 509–514 (2007).

32. Canadian Coast Guard. Ice Navigation in Canadian Waters. Tech. Rep., Government of Canada, Ottawa (2012).
33. Wang, J., Mysak, L. & Grant-Ingram, R. Interannual variability of sea-ice cover in hudson bay, baffin bay and the Labrador sea. *Atmosphere* **32**, 421–447 (1994).
34. Mysak, L. & Power, S. Sea-ice anomalies in the western Arctic and Greenland-Iceland Sea and their relation to an interdecadal climate cycle. *Climat. Bull.* **26**, 147–176 (1992).
35. Mysak, L., Manak, D. & Marsden, R. Sea-ice anomalies observed in the Greenland and Labrador seas during 1901-1984 and their relation to an interdecadal Arctic climate cycle. *Clim. Dyn.* **5**, 111–133 (1990).
36. Bunn, A. A dendrochronology program library in R (dplR). *Dendrochronologia* **26**, 115–124 (2008).
37. Leavitt, S. W. & Danzer, S. R. Method for batch processing small wood samples to holocellulose for stable-carbon isotope analysis. *Anal. Chem.* **65**, 87–89 (1993).
38. McKenney, D. W. et al. Customized spatial climate models for North America. *Bull. Am. Meteorol. Soc.* **92**, 1611–1622 (2011).
39. Conrad, V. Usual formulas of continentality and their limits of validity. *Eos Trans. Am. Geophys. Union* **27**, 663–664 (1946).
40. Rayner, N. A. Global analyses of sea surface temperature, sea ice, and night marine air temperature since the late nineteenth century. *J. Geophys. Res.* **108**, 4407 (2003).
41. Schmidt, G. A. et al. Configuration and assessment of the GISS ModelE2 contributions to the CMIP5 archive. *J. Adv. Model. Earth Syst.* **6**, 141–184 (2014).
42. Schmidt, G. A., LeGrande, A. N. & Hoffmann, G. Water isotope expressions of intrinsic and forced variability in a coupled ocean-atmosphere model. *J. Geophys. Res.* **112**, 10103 (2007).
43. Stein, A. F. et al. NOAA's HYSPLIT atmospheric transport and dispersion modeling system. *Bull. Am. Meteorological Soc.* **96**, 2059–2077 (2015).
44. Kalnay, E. et al. The NCEP/NCAR 40-year reanalysis project. *Bull. Am. Meteorol. Soc.* **77**, 437–472 (1996).
45. Misson, L. MAIDEN: a model for analyzing ecosystem processes in dendroecology. *Can. J. Forest Res.* **34**, 874–887 (2004).
46. Danis, P. A., Hatté, C., Misson, L. & Guiot, J. MAIDENiso A multiproxy biophysical model of tree-ring width and oxygen and carbon isotopes. *Can. J. Forest Res.* **42**, 1697–1713 (2012).
47. de Mendoza, I. et al. A new snow module improves predictions of the isotope-enabled MAIDENiso forest growth model. *Geosci. Model Dev.* **15**, 1931–1952 (2022).
48. Keeling, C. D. et al. Atmospheric carbon dioxide variations at Mauna Loa Observatory, Hawaii. *Tellus* **28**, 538 (1976).
49. Peters, W. et al. An atmospheric perspective on North American carbon dioxide exchange: CarbonTracker. *Proc. Natl Acad. Sci.* **104**, 18925–18930 (2007).
50. R Core Team. R: A Language and Environment for Statistical Computing. (R Foundation for Statistical Computing, Vienna, Austria, 2023). https://www.R-project.org/.

Acknowledgements

The authors would like to thank Jean-François Hélie and Agnieszka Adamowicz from the Geotop's stable isotopes laboratory, for their help with laboratory analyses. The authors would also like to thank Dominique Arseneault (Université du Qubec à Rimouski) for constructive comments during earlier stage of this paper. This work was supported by the Natural Sciences and Engineering Research Council of Canada (NSERC) through grant Nos. RGPIN 2016-05244, RGPIN 2021-04216, and CRDPJ 485475 - 2015, to Étienne Boucher.

Author contributions

J.L., E.B. and A.d.V. conceived the analysis and sampling design. J.L. and E.B. performed the field work. J.L. performed laboratory analyses at the GEOTOP laboratory of Université du Québec à Montréal. J.L., E.B., A.d.V. I.H.d.M., F.G., A.L., L.A.H., and R.d.F. contributed to the analysis of isotopic chronologies. J.L. and E.B. contributed to the writing of the paper. All authors (J.L., E.B., A.d.V. I.H.d.M., F.G., A.L., L.A.H., and R.d.F.) reviewed and edited the paper. E.B., I.H.d.M. and F.G. performed MAIDENiso experiments. R.d.F. performed ModelE computations and $\delta^{18}O_p$ calculations. E.B. performed HYSPLIT analysis. E.B. acquired the funding for this study.

Competing interests

Aliénor Lavergne is an Editor for Communications Earth & Environment, but was not involved in the editorial review of, nor the decision to publish this article. The remaining authors declare no competing interests.

Additional information

Supplementary information The online version contains supplementary material available at https://doi.org/10.1038/s43247-024-01271-4.

Correspondence and requests for materials should be addressed to Étienne Boucher.

Peer review information *Communications Earth & Environment* thanks the anonymous reviewers for their contribution to the peer review of this work. Primary Handling Editor: Joe Aslin. A peer review file is available.